

Microbial food web structure in a naturally iron-fertilized area in the Southern Ocean (Kerguelen Plateau)

U. Christaki^{a,*}, I. Obernosterer^b, F. Van Wambeke^c, M. Veldhuis^d, N. Garcia^e, P. Catala^b

^aLaboratoire d'Océanologie et de Géosciences (LOG) CNRS – UMR 8187, Université du Littoral Côte d'Opale, 32 avenue Foch, 62930 Wimereux, France

^bLaboratoire d'Océanographie Biologique de Banyuls (ARAGO) CNRS UMR 7621, Université Pierre et Marie Curie-Paris 6, 66650 Banyuls-sur-Mer, France

^cLaboratoire de Microbiologie, Géologie et Ecologie Marine (LMGEM), CNRS, Université de la Méditerranée, UMR 6117, Campus de Luminy, Case 901, 13288 Marseille cedex 9, France

^dRoyal Netherlands Institute for Sea Research, P.O. Box 59, 1790 AB, Den Burg, Texel, The Netherlands

^eLaboratoire d'Océanographie et de Biogéochimie, OSU/Centre d'Océanologie de Marseille, Campus de Luminy, Aix-Marseille Université, CNRS, LOB-UMR 6535, case 901, 13288 Marseille cedex 9, France

Accepted 14 December 2007

Available online 10 March 2008

Abstract

The objective of this study in the framework of the Kerguelen Ocean and Plateau compared Study, 2005–2007 (KEOPS) project was to examine the microbial food web structure within a phytoplankton bloom induced by natural iron fertilization. Integrated bacterial production (BP, 0–100 m) varied 12-fold over the study area (23.5–304 mg C m⁻² d⁻¹), while bacterial abundance (0–100 m) varied only by a factor of 2.8. Highest bacterial abundances and rates of BP were observed in the center of the diatom-dominated bloom, and substantial decreases in BP towards the later bloom stage were detectable. The abundance of bacterial predators (heterotrophic nanoflagellates, HNF) showed a significant coupling with BP in the high-nutrient low-chlorophyll (HNLC) area only. In the core of the bloom, BP consumed by HNF was 27%, 29%, 52% and 34% during the four consecutive visits that extended over 4 weeks and was much higher (80–95%) in HNLC waters. The relative contribution of the small-sized (<10 μm) phytoplankton in terms of chlorophyll was only minor within bloom. Ciliated protozoa showed low abundance (20–556 cells l⁻¹) all over the studied area; however, in terms of biomass ciliates were more important within (224 mg C m⁻², 0–100 m) than outside the bloom (30.5 mg C m⁻², 0–100 m). This difference was attributable mainly to tintinnids *Cymatocyclis* spp. accounting for 30–80% of the total ciliate biomass within the Kerguelen bloom but being rare in the HNLC water. Mixotrophic ciliate biomass accounted for 40–60% of the total aloricate ciliate biomass all over the studied area. This was mainly due to the relatively large size of mixotrophic ciliates present in the samples (*Tontonia antarctica*, *Strombidium* spp. and *Laboea strobila*). Overall, our results suggest a strong response of bacteria, weak response of HNF, and strong controlling effects on ciliates. The weak coupling between heterotrophic bacteria and HNF and the low abundance of ciliates suggest a low transfer of carbon from the microbial to the classical food web within the Kerguelen bloom.

© 2008 Elsevier Ltd. All rights reserved.

Keywords: Southern Ocean; Iron fertilization; Microbial food web

1. Introduction

Considerable effort has been made over the last decade towards the understanding of the relationship between phytoplankton biomass and productivity and iron availability particularly in the Southern Ocean, the largest high-

nutrient low-chlorophyll (HNLC) region. Several recently performed iron addition experiments have clearly demonstrated that iron is the primary limiting factor for phytoplankton growth over large parts of the Southern Ocean (Boyd et al., 2000; Gervais et al., 2002; Coale et al., 2004; reviewed in Boyd et al., 2007). With respect to the trophic organization, HNLC areas seem conceptually similar to oligotrophic regions dominated by small producers and an efficient microbial food web (Landry

*Corresponding author. Tel.: +33 3 21 99 64 35; fax: +33 3 21 99 64 00.

E-mail address: Christaki@univ-littoral.fr (U. Christaki).

et al., 1997). Upon iron-addition, however, a pronounced shift to larger phytoplankton cells, in particular diatoms has been observed. While evidence for iron limitation of phytoplankton growth is unequivocal, the subsequent direct or indirect impact of iron on heterotrophic components of the microbial food web is less clear.

Heterotrophic bacteria and microzooplankton also have significant Fe demands (Tortell et al., 1996; Strzepek et al., 2005); they are thus potential competitors with phytoplankton when Fe resources are limited (Maldonado and Price, 1999). It also has been demonstrated that the microbial foodweb plays a key role in rapidly recycling much of the Fe required by plankton in the upper ocean (Strzepek et al., 2005 and references therein). The few studies examining iron limitation on the different components of the microbial food web conclude that Fe enrichment affects heterotrophic bacteria, either directly by the alleviation of Fe limitation (Pakulski et al., 1996; Arrieta et al., 2004) or indirectly through enhanced phytoplankton growth and the subsequent increasing supply of dissolved organic matter (Cochlan, 2001; Hall and Safi, 2001). This latter hypothesis is confirmed by experiments showing that C rather than Fe is the primary limiting nutrient for heterotrophic bacteria in low-iron waters (Church et al., 2000; Kirchman et al., 2000).

From results obtained during IronEx II, Landry et al. (2000a, b) suggested that microzooplankton had the potential to graze diatoms and these authors concluded that iron fertilization decreases the efficiency of carbon sequestration to the deep ocean, an idea also maintained by Saito et al. (2005) for SEEDS. However, only a moderate increase in microzooplankton biomass was observed during mesoscale Fe-fertilization experiments (Landry et al., 2000b; Hall and Safi, 2001), and the microzooplank-

ton grazing pressure on the total phytoplankton community decreased (Saito et al., 2005; Boyd et al., 2004) or affected mainly the small-sized phytoplankton population, e.g., autotrophic nanoflagellates (Hall and Safi, 2001).

Satellite observations over a number of years have clearly identified a zone rich in chlorophyll during summer months associated with the Kerguelen Continental Shelf, within the otherwise HNLC Southern Ocean. The central hypothesis of the Kerguelen Ocean and Plateau compared Study, 2005–2007 (KEOPS) project was that enhanced vertical mixing of deep iron-rich water above the plateau sustained these phytoplankton blooms (Blain et al., 2001). The extent and the duration of the Kerguelen bloom (roughly 3 months) allowed a comprehensive study on natural iron fertilization of the Southern Ocean and a detailed comparison to previous short-term (weeks) mesoscale iron additions.

The objective of the present study was to examine the microbial food web structure associated with the Kerguelen bloom. To determine the impact of natural iron fertilization on microbial food web processes, we investigated the abundances and production of autotrophic (phytoplankton <math><10\ \mu\text{m}</math>) and heterotrophic (bacteria, flagellates and ciliates) components and their predators within the Kerguelen bloom and in typical HNLC waters.

2. Methods

2.1. Sampling strategy

This study was carried out during the KEOPS-cruise from 19 January to 13 February 2005. Water samples were collected from 18 stations situated on three transects (A, B and C, Fig. 1) covering the bloom area above the

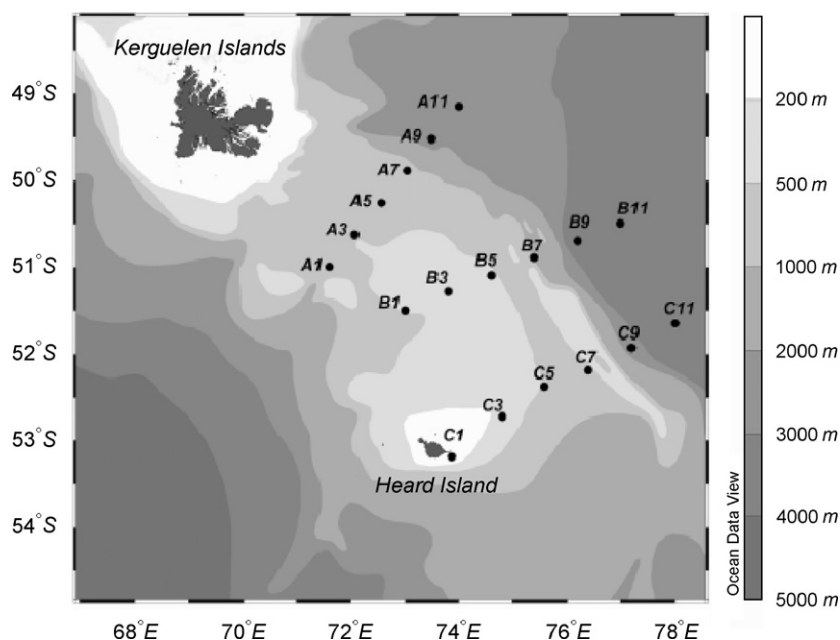


Fig. 1. Bathymetry of the study area and location of the sampled stations.

Kerguelen Plateau (Blain et al., 2008) and the ocean zone with HNLC conditions. Satellite images during the KEOPS cruise (MODIS results provided by CSIRO marine research, images presented in Blain et al., 2007) showed that station A3 was the core of the bloom, stations A1, A5, B1, B3 and B5 were influenced by the bloom, and stations, A7–A11, B7–B11 and the whole transect C were HNLC stations. Thus, during the KEOPS cruise the stations A3 (50°38'S, 72°05'E) and C11 (51°39'S, 78°00'E, Fig. 1) were considered as the two most contrasting stations and were visited several times over a period of 1 month. Here we present data from four visits at station A3 (Table 1) and one visit at station C11. Water samples were collected with 12-l Niskin bottles mounted on a CTD rosette. Sampling for microbial parameters was performed at standard depths (5, 10, 20, 40, 60, 80, 100, 125, 150 and 200 m) except for ciliates (5, 10, 20, 40, 60, 80 and 100 m). Bacterial production (BP), abundance and pico- and nanophytoplankton were measured at all stations (three transects, 18 stations). Heterotrophic nanoflagellate and ciliate abundance and grazing on bacteria were measured at seven to eight selected stations representing bloom and HNLC conditions (detailed in Table 1). For the presentation of data in this paper, we present whole profiles in figures, while mean values are calculated within the mixed layer (Zm) and integrations are all 0–100 m layer to allow comparison between stations.

Table 1
Sampling dates and station positions for parameters presented in this paper

Station	Date (2005)	Longitude	Latitude	Parameters
A3-1	19/01	50°37.85'S	72°04.26'E	1, 2, 3, 4, 5, 6, 7
A11	20/01	49°09.90'S	73°59.50'E	1, 2, 3, 4 ^a , 5, 6
A9	21/01	49°31.52'S	73°30.30'E	1, 2, 5
A7	22/01	49°53.40'S	73°02.28'E	1, 2, 5
A5	22/01	50°15.72'S	72°34.12'E	1, 2, 5
A1	23/01	51°00.08'S	71°35.87'E	1, 2, 3, 4, 5
A3-3	24/01	50°37.85'S	72°04.26'E	1, 2, 3, 4, 5, 6, 7
C11-1	26/01	51°37.40'S	77°57.30'E	1, 2, 4 ^a , 5, 6
B11	29/01	50°30.40'S	76°59.00'E	1, 2, 4 ^a , 5
B9	30/01	50°41.90'S	76°12.00'E	1, 2, 5
B7	30/01	50°53.63'S	75°23.57'E	1, 2, 5
B5	01/02	51°06.10'S	74°36.00'E	1, 2, 3, 4, 5, 6, 7
B3	02/02	51°17.98'S	73°58.09'E	1, 2, 5
B1	02/02	51°30.00'S	73°00.00'E	1, 2, 4, 5
A3-4	04/02	50°37.85'S	72°04.26'E	1, 2, 3, 4, 5, 6, 7
C9	06/02	51°55.40'S	77°11.92'E	1, 2, 4 ^a , 5
C7	07/02	52°11.40'S	76°23.70'E	1, 2, 4 ^a , 5
C5	07/02	52°22.80'S	75°35.00'E	1, 2, 3, 4 ^a , 5, 7
C3	08/02	52°42.86'S	74°47.93'E	1, 2, 4 ^a , 5
C1	09/02	53°10.86'S	73°52.63'E	1, 2, 4 ^a , 5, 7
A3-5	12/02	50°37.85'S	72°04.26'E	1, 2, 3, 4, 5, 6, 7

1, heterotrophic bacteria; 2, bacterial production; 3, heterotrophic nanoflagellates; 4, ciliates; 5, phototrophic pico- and nanoplankton; 6, grazing experiment of bacteria by HNF; 7, fractionated primary production.

^aSurface values only (5–10 m).

2.2. Sampling and counting of bacteria

Seawater samples (3-ml) were preserved with 2% formaldehyde (final concentration), quick-frozen in liquid nitrogen and stored at -80°C until flow cytometric analysis described in detail in Obernosterer et al. (2008). Briefly, before counting, samples were stained with SYBR-Green I (0.025% (vol/vol) final concentration, Molecular Probes). Heterotrophic bacterial counts were performed with a FACSCalibur flow cytometer (Becton Dickinson) according to Lebaron et al. (1998, 2001). Regions were established on cytogram plots of side scatter versus green fluorescence to define high nucleic acid (HNA) and low nucleic acid (LNA) cells. Abundance was converted to biomass using a carbon conversion factor of $12.4\text{ fg C cell}^{-1}$ (Fukuda et al., 1998).

2.3. Bacterial production

BP was estimated by the ^3H -leucine method at nine depths in the 0–200 m water column. At each depth, 1.5-ml duplicate samples and a control were incubated with a mixture of L-[4,5- ^3H]leucine (Amersham, 160 Ci mmol^{-1}) and non-radioactive leucine added at final concentrations of 7 and 13 nM, respectively, for the upper 100 m, and 13 and 7 nM, respectively, for the 100–200-m depth layer. Samples were incubated and treated following the microcentrifugation protocol (Smith and Azam, 1992) as described in detail in Van Wambeke et al. (2002). Samples were incubated in the dark at the ambient temperature of the depth where samples were collected. The incubation time (2–3 h) was tested to satisfy linear incorporation with time. We checked by concentration kinetics (2.5, 5, 10, 20 and 40 nM), at three stations inside and outside the bloom at 5 and 175 m depths that there was no isotopic dilution and thus, used a conversion factor after Kirchman (1993) of $1.55\text{ kg C mol}^{-1}$ leucine incorporated.

2.4. Heterotrophic bacterial grazing measurement

Four grazing experiments were performed at station A3, and at stations A11, B5 and C11 one grazing experiment was performed each (Fig. 1, Table 1). Seawater for these experiments was collected in the surface mixed layer at 10 or 20 m. Duplicate bottles (50 ml) were inoculated with $0.5 \times 10^5\text{ ml}^{-1}$ FLB (monodispersed Fluorescently Labeled Bacteria in our case 'minicells' *E. coli* strain x1488 provided by the Yale University Genetic Stock). FLB were prepared according to Sherr et al. (1987) modified by Pace et al. (1990). We determined flagellate ingestion in sub-samples from 15 and 30 min. Ingestion rate on bacteria ($\text{bact HNF}^{-1}\text{ h}^{-1}$) was then calculated by multiplying the ingestion rate of FLB by the ratio of bacteria to added FLB (Sherr et al., 1987; Pace et al., 1990).

2.5. Sampling and counting of ciliated protozoa and heterotrophic nanoflagellates (HNF)

For ciliate enumeration, duplicate samples (250 ml) were taken from the upper 100 m at different increments (5, 10, 20, 30, 40, 50, 60, 80 and 100 m) at stations A3, C11 and B5 (Fig. 1, Table 1). Surface samples (5 or 10 m) were also taken at stations A1, B11, C1, C3, C5, C7 and C9 (Fig. 1, Table 1). One 250-ml sample was fixed with acid Lugol's solution in order to obtain final concentrations of 2% for quantitative counts, and the other with particle free borax-buffered 37% formaldehyde for distinction of the trophic status of the ciliate—heterotroph or mixotroph. The samples were then stored at 4 °C in the dark until analysis (3–6 months).

In the laboratory, the 250-ml samples were left to settle for 3–4 days at 4 °C. Before examination the top was gently siphoned off using a low vacuum pump. The bottom 100 ml of the sample were transferred into Hydro-Bios Kiel combined plate settling chambers allowing it to settle for a minimum of 16 h and then examined with an Olympus IX-70 inverted microscope at $\times 400$ magnification. The microscope was equipped for transmitted light, phase-contrast and epifluorescence microscopy. Blue light excitation (DM 500-nm dichroic mirror, BP 450–480-nm exciter filter, BA 515-nm barrier filter, and a 100-W mercury burner) was used to detect chlorophyll autofluorescence and to distinguish plastidic from non-plastidic ciliates. Lugol's fixed samples were enumerated and sized with phase contrast while borated-formalin fixed samples were examined using epifluorescence microscopy.

All ciliates in each sample were counted and were classified as plastidic (mixotrophs) or aplastidic on the basis of genus and by the presence of an autofluorescence signal. Aplastidic and mixotrophic ciliates were differentiated into aloricate (naked ciliates comprising taxa of Oligotrichida and Choreotrichida) and tintinnids (order Choreotrichida, suborder Tintinnina, Montagnes and Lynn, 1991). Ciliates were grouped into four size groups (Table 2) and were identified wherever possible to the species level based on Petz (2005). Biovolumes of all taxa and morphotypes identified in this study were calculated using the linear dimensions of cells. A total of 400 cells belonging to 25 species/categories were sized in different samples. Linear dimensions (length and diameter) were measured at $\times 400$ magnification using an image analyzer

with a camera mounted on the microscope. Equations for a sphere, prolate spheroid or cone were applied depending on cell shape. Oral membranelles and tail structures were not included in the estimation of cell geometry (Stoecker et al., 1994). Biovolumes were converted to biomass using volume-to-carbon conversion factors of $190 \text{ fg C } \mu\text{m}^{-3}$ for Lugol's preserved samples (Putt and Stoecker, 1989). Ciliates were further divided into four size groups; because of the different shapes of ciliates these size groups refer to ESD (equivalent spherical diameter, Table 2) calculated from the biovolume of the cells (e.g., a conical cell with dimensions $30 \times 50 \mu\text{m}$, has an ESD of approximately $28.23 \mu\text{m}$). Empty tintinnid loricas were counted separately and were not included in abundance and biomass calculations. For tintinnid biovolumes, linear dimensions of the lorica were measured and 30% cell occupancy was considered (Gilron and Lynn, 1989). However, small tintinnids appeared to occupy a greater percentage of the lorica and 50% cell occupancy was assumed (Beers and Stewart, 1967).

To enumerate HNF, 20–30-ml samples were preserved with formaldehyde at a final concentration of 2%. Samples were kept at 4 °C in the dark, filtered on black Nuclepore filters (pore size: $0.8 \mu\text{m}$), stained with DAPI (Porter and Feig, 1980) within a few hours of sampling, and stored at $-20 \text{ }^\circ\text{C}$ until counting. HNF were enumerated using a LEITZ DMRB epifluorescence microscope at $1000 \times$. In order to distinguish between autotrophic and HNF, autofluorescence (chlorophyll) was determined under blue light excitation. To quantify the biomass of HNF, linear dimensions of a total of 350 cells were measured using an ocular micrometer. The average biovolume of HNF was $22.5 \mu\text{m}^3$ (equivalent to an ESD $\approx 3.5 \mu\text{m}$). Biovolumes were converted to biomass using a conversion factor of $220 \text{ fg C } \mu\text{m}^{-3}$ (Børsheim and Bratbak, 1987). Abundance and biomass standing stocks were calculated by the integration of sampling depths between 0 and 100 m.

2.6. Sampling and counting of autotrophic pico- and nanophytoplankton

Freshly collected CTD bottle samples were routinely analyzed for their phytoplankton community composition with a bench-top flow cytometer (COULTER XL-MCL) usually within 1 h after sampling. Prior to analysis the samples were stored on ice in the dark. Chlorophyll *a* (Chl *a*) autofluorescence (emission $> 630 \text{ nm}$) and phycoerythrin autofluorescence (PE, emission $575 \pm 20 \text{ nm}$) were measured next to the forward scatter (indicator of cell size). The machine drift was tested using calibration beads with known size (3 and $10 \mu\text{m}$) and fluorescence signals on a day-to-day basis (Veldhuis and Kraay, 2000). The phytoplankton community showed a continuous range of cell size versus cellular Chl *a* autofluorescence but in general three to five major groups could be distinguished with a cell size $< 30 \mu\text{m}$. Autotrophic cells $< 10 \mu\text{m}$, possible preys of microzooplankton and belonging in the microbial food

Table 2
Ciliate size classes

ESD size class (μm)	Biovolume ($10^3 \mu\text{m}^3$)	Volume class (μm^3)
10–20	0.5–4	10^2 – 10^3
20–30	4–14	10^3 – 10^4
30–50	14–65	10^3 – 10^4
50–100	65–500	10^4 – 10^5

ESD: equivalent spherical diameter.

web, are considered in this paper. Estimated spherical diameters and related biovolume were calculated as described in Veldhuis and Kraay (2000), applying fractionated filtration steps (10, 8, 5, 3, 2, 1 and 0.6 μm). Phytoplankton groups differed in cell size and included picophytoplankton (<2 μm), small-sized eukaryotes and occasionally also low numbers of small coccolithophorids (based on the presence of high scatter signals—not presented here). Cell carbon was estimated using the empirical relationship between biovolume and cell carbon of Verity et al. (1992).

$$0.433 \times (\text{BV})^{0.863}, \quad (1)$$

where BV is biovolume in μm^3 and based on the ESD for each group and each sample and cell carbon is expressed in pg C cell^{-1} .

2.7. Phytoplankton biomass and production

Total Chl *a* (Chl *a* and divinyl-Chl *a*) was measured by high performance liquid chromatography (HPLC, Van Heukelem and Thomas, 2001). Rates of primary production were determined at six light levels using ^{13}C incorporation (Slawyk et al., 1997). Samples were incubated for 24 h on deck in incubators equipped with nickel screens simulating light intensity from 100% to 1%. Temperature in the incubators was maintained by a constant surface water flow. Size fractionation performed immediately after incubation experiments allowed estimating the contribution of the <10- μm size fraction to total primary production. The isotopic enrichment analysis was performed on an Integra-CN PDZ EUROPA mass spectrometer calibrated with glycine references every batch of 10–15 samples. The accuracy of the analytical system was also regularly verified using reference materials from the International Atomic Energy Agency (IAEA, Analytical Quality Control Services).

3. Results

3.1. Study site

Hydrographic conditions during KEOPS are reported in detail in Park et al. (2008). As revealed by physical data the same water mass was sampled at station A3 during the four visits. The wind mixed-layer depth in the KEOPS area ranged from 44.3 m (station A11) to 128.5 m (station C1). Mean water temperature in the wind mixed layer was 3.5 and 1.8 $^{\circ}\text{C}$ in the northern and southern part, respectively (stations A3 and C11, Fig. 2). The macronutrient concentration over the first 100 m of the water column varied little during the study period and was on average $26.7 \pm 3.1 \mu\text{M}$ nitrate plus nitrite and $1.8 \pm 0.3 \mu\text{M}$ phosphate (all stations pooled, Mosseri et al., 2008). Average silicic acid concentrations were 2.1 ± 1.0 and $25.1 \pm 0.7 \mu\text{M}$ in the bloom and in the HNLC area, respectively, Mosseri et al., 2008). In surface water, dissolved iron (DFe) was

$\approx 0.1 \text{ nM}$ at all stations, but increased with depth in the bloom area (Blain et al., 2008). The large phytoplankton bloom, which was dominated by large diatoms, was sustained by the supply of iron and major nutrients to surface waters from iron-rich deep water over the Kerguelen Plateau. Availability of iron in surface waters over the plateau appears to be enhanced by, both the greater winter stock and a higher ongoing supply from increased vertical mixing and the steeper DFe gradient (detailed in Blain et al., 2007). The bottom of the euphotic layer (depth of 1% surface PAR) varied between 41 and 58 m in the bloom area (station A3) and between 97 and 113 m at the HNLC area (station C11). The bloom formation started in early November and collapsed in late February (MODIS satellite images).

3.2. Bacterial abundance and production in relation to phytoplankton biomass

Bacterial abundance ranged from 0.99 to $7.8 \times 10^5 \text{ cells ml}^{-1}$ (B11, 200 m and A3-3, 60 m). The highest integrated bacterial abundance (0–100 m) was observed at A3-3 station ($64.4 \times 10^{12} \text{ cells m}^{-2}$) and the lowest at C11 station ($23.2 \times 10^{12} \text{ cells m}^{-2}$). Integrated bacterial biomass ranged from 287 to 797 mg C m^{-2} in the 0–100 m layer (C11 and A3-3 stations, respectively). BP revealed large variability across the sampling sites, with values ranging between 0.9 and 176 $\text{ng C l}^{-1} \text{ h}^{-1}$ (C7 at 10 m and A3-1 at 80 m, Figs. 3 and 4). Integrated (BP, 0–100 m) varied 12-fold over the studied area (from 23.5 $\text{mg C m}^{-2} \text{ d}^{-1}$ at C3 to 304 $\text{mg C m}^{-2} \text{ d}^{-1}$ at A3-1). By contrast, integrated bacterial abundance varied over a much narrower range (by 2.8-fold) between stations and depths. Integrated TChl *a* (0–100 m) varied 11.4-fold over the studied area and ranged between 16.1 and 183.9 mg Chl a m^{-2} (stations B11 and A1, respectively). Bacterial biomass and production were significantly correlated with chlorophyll (Chl *a*, $r = 0.605$, $n = 179$, $p < 0.0001$ and $r = 0.600$, $n = 178$, $p < 0.0001$, respectively).

3.3. Abundance and biomass of HNF in relation to BP

The standing stock of HNF showed small variability across sites, ranging from 7.5 to $19.4 \times 10^{10} \text{ cells m}^{-2}$ (0–100 m) (Fig. 4, Table 3). HNF integrated biomass (0–100 m) ranged from 370 to 962 mg C m^{-2} (at stations A3-5 and B5, respectively). HNF abundance was significantly related to BP ($r = 0.37$, $n = 70$, $p = 0.002$). Interestingly, when considering this correlation for BP values <55 $\text{ng C l}^{-1} \text{ h}^{-1}$ (measured outside the bloom area) the correlation was stronger ($r = 0.68$, $n = 44$, $p < 0.0001$), while for BP values >55 $\text{ng C l}^{-1} \text{ h}^{-1}$ (measured at stations A1, A3, A5, B1 and B3 associated with the diatom bloom, cf. Fig. 3) the correlation between BP and HNF was not significant ($p = 0.1$).

Grazing experiments yielded ingestion rates of 1.8–2.6 $\text{bact HNF}^{-1} \text{ h}^{-1}$ at station A3 and A11 (mean

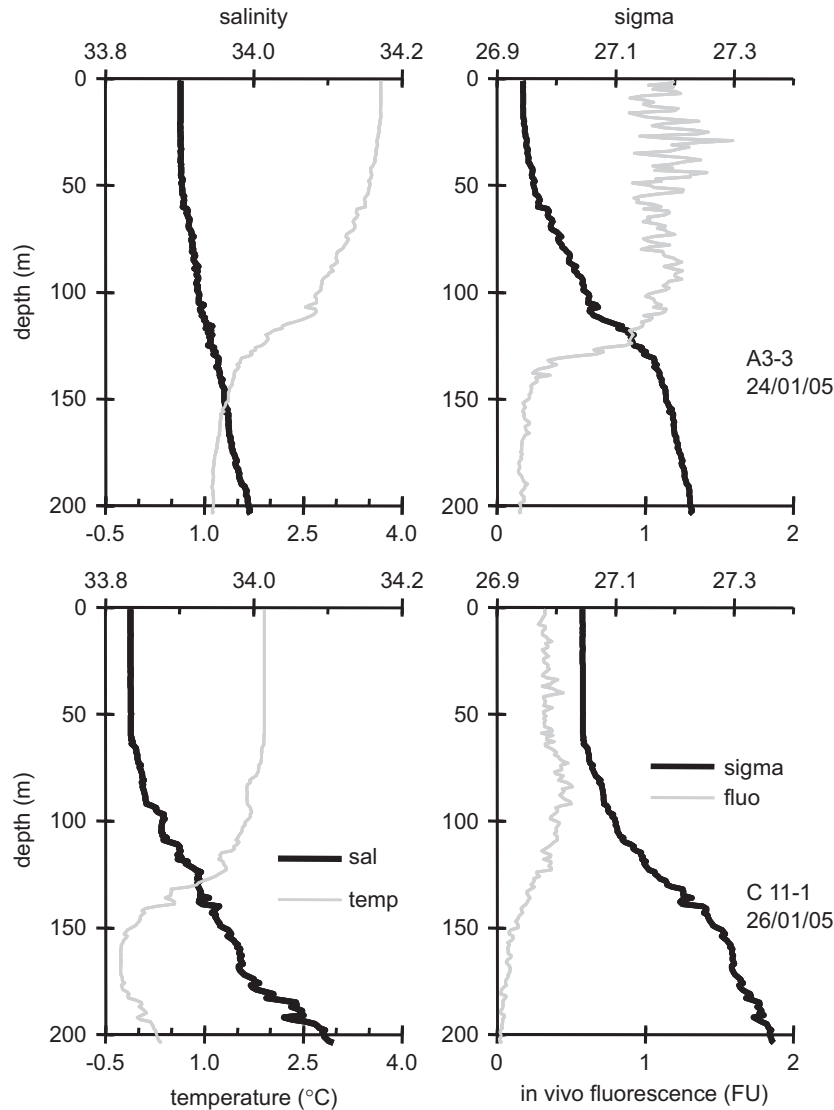


Fig. 2. Representative profiles of salinity (sal), temperature (temp, °C), sigma theta (kg m^{-3}) and Chl *a* ($\mu\text{g l}^{-1}$) as derived from *in vivo* fluorescence depth profiles within the bloom (A3-station) and the HNLC area (C11-station).

2.1 $\text{bact HNF}^{-1} \text{h}^{-1}$) and 0.8–2 $\text{bact HNF}^{-1} \text{h}^{-1}$ at stations C5, C11 and B5 (mean 1.5 $\text{bact HNF}^{-1} \text{h}^{-1}$). Based on these subsurface grazing measurements and the abundances of heterotrophic bacteria and HNF in the mixed layer, an integration of bacterial consumption in the mixed layer was estimated. This estimation showed higher bacterial mortality due to HNF at the HNLC stations than in the bloom area. HNF consumed 27%, 29%, 52% and 34% of the BP during the four consecutive visits at station A3 and 80%, 83%, 95% and 83% at stations B5, C5, C11 and A11, respectively.

3.4. Ciliated protozoa

Ciliate abundance was generally low ranging from 20 to 556 cells l^{-1} , and no major differences between stations inside and outside the bloom were detectable. It is worthy to note that ciliate abundance increased with depth in the

bloom area showing maximum abundances between 80 and 100 m (A3-1, A3-3, A3-4 and B5) while at stations A3-5 and C11 ciliate abundances were more or less constant throughout the 0–100 m water column (Fig. 4). In terms of ciliate biomass distinct differences between stations A3 and C11 were detectable (Fig. 5). Ciliate biomass integrated over the 0–100 m water column ranged from 30.5 to 224 mg C m^{-2} (stations C11 and A3-3, respectively, Fig. 5A and B). The highest ciliate biomass was recorded at station A3-3 due to an increase of tintinnids (Table 3, Fig. 5A).

The mixotrophic biomass accounted for 40–60% of the aloricate ciliate biomass over the studied area (Fig. 5A). This can be explained by the relatively large size of mixotrophic ciliates present above the Kerguelen Plateau (*Tontonia antarctica*, *Strombidium antarcticum*, *Strombidium conicum* and *Laboea strobila*, belonging to the $\text{ESD} = 30\text{--}50 \mu\text{m}$ size class, Table 2, Fig. 5B). The most abundant mixotrophic species present in all samples was

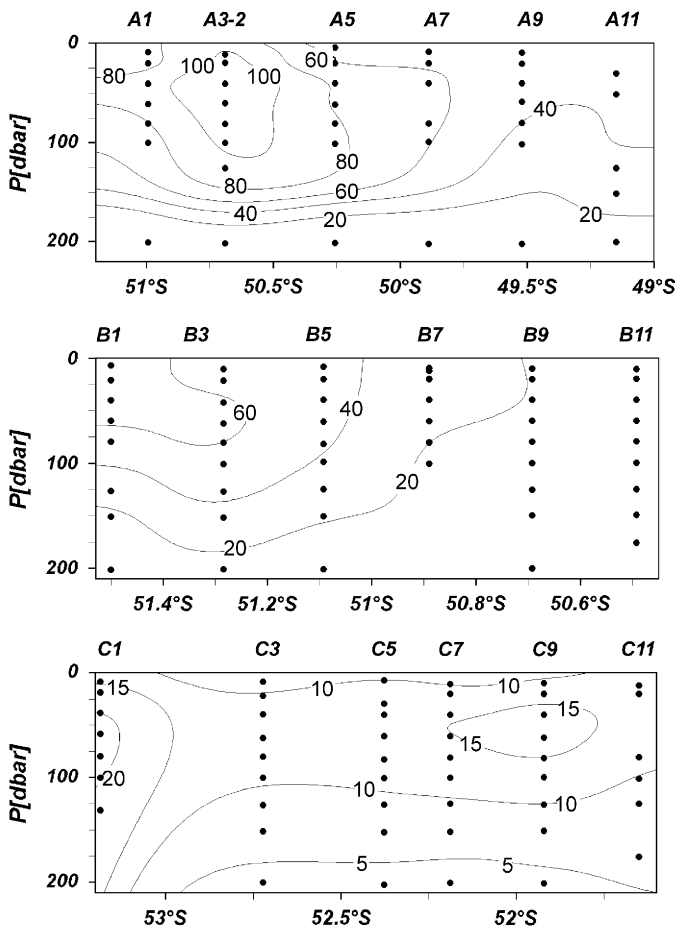


Fig. 3. Bacterial production ($\text{ng C l}^{-1} \text{h}^{-1}$) in the upper 200 m along the transects A, B and C (cf. Fig. 1 and Table 1). Interpolation between sampling points in contour plots was made with Ocean Data View program (VG gridding algorithm, Schlitzer, 2004).

T. antarctica (maximum abundance 156 cells l^{-1} at station C5, depth of 10 m). Tintinnid biomass (loricate ciliates) accounted for 30–80% of the total ciliate biomass within the bloom (stations A3 and B5), while it represented only 1% of the total ciliate biomass at C11 (Fig. 5A). The largest and most abundant tintinnid taxa present in most samples were *Cymatocylis calyciformis* and *Cymatocylis vanhoeffeni*, tintinnid species accounting for the biomass maximum at station A3-3 (max abundance 100 cells l^{-1} at A3-3 at 60 and 80 m). The smaller species *Salpingella* spp., while not as important in biomass, was present in most samples. Other tintinnid belonging to the genera *Undella*, *Codonellopsis*, *Cymatocylis*, and *Coxiella* occurred sporadically in the samples.

Nauplii and copepodites were present in all samples with a proportion of about 1 copepod to 4–5 ciliate at stations C11 and A3 and about 1 copepod to 9 ciliates at station B5 (Fig. 5D).

3.5. Pico- and nanophytoplankton

The standing stock of phototrophic nanoplankton (PNAN, 2–10 μm) ranged between 5 and $33 \times 10^{10} \text{ cells m}^{-2}$

over the 0–100 m layer (at stations A3-1 and C5, respectively). PNAN integrated biomass (0–100 m) ranged from 430 to 2402 mg C m^{-2} (at stations B5 and C5, respectively) (Fig. 6 A). Autotrophic picophytoplankton (<2 μm , pro- and eukaryotes) abundances and biomasses were low ranging from 0.5 to $11 \times 10^{10} \text{ cells m}^{-2}$ and from 2 to 113 mg C m^{-2} (at stations A3-3 and C5, respectively, Fig. 6A). The percentage of primary production in the <10 μm generally followed phototrophic phytoplankton biomass variation (Table 4) and varied from 17% to 38% of total PP at station A3 to 86% at station C11. The ratio of heterotrophic versus autotrophic biomass within the microbial food web was from 0.3 to 3.4 (stations C5 and B5, respectively), this ratio was 1.3, 2.2, 0.6 and 1.4 during the subsequent visits at station A3 (Fig. 6A and B).

4. Discussion

The results reported here demonstrate that the microbial food web is quantitatively and qualitatively altered within a phytoplankton bloom induced by natural iron fertilization of the Southern Ocean. Heterotrophic bacteria and ciliated protozoa revealed distinct features within the Kerguelen bloom, while the response of other components of the microbial food web such as HNF and small-sized phytoplankton was far less pronounced. The potential consequences on the cycling of carbon are discussed below.

The firm response of heterotrophic bacteria, particularly in terms of biomass production, to the Kerguelen bloom confirms observations from mesoscale iron-addition experiments (Hall and Safi, 2001; Arrieta et al., 2004; Oliver et al., 2004; Cochlan, 2001; reviewed in Boyd et al., 2007) (Table 5). The increase in bacterial abundance and production within the Kerguelen bloom is, however, substantially higher (by a factor of 2.8 and 12, respectively) than previously reported (Table 5). Interestingly, HNA-containing cells dominated ($81 \pm 3\%$ of total bacterial abundance) the heterotrophic bacterial community associated with the Kerguelen bloom, while the relative contribution of HNA-cells was much smaller in HNLC-waters ($48 \pm 4\%$ of total bacterial abundance; Obernosterer et al., 2008). The correlation of BP with total bacterial abundance was significant ($r = 0.654$, $n = 145$, $p < 0.0001$), however, the correlation of BP considering only HNA numbers was even stronger ($r = 0.771$, $n = 145$, $p < 0.0001$), suggesting that HNA cells were mainly responsible for the high BP above the Kerguelen Plateau (Obernosterer et al., 2008).

Despite the dramatic differences in BP between the bloom area and the HNLC areas, our data showed that bacterial biomass varied within a relatively narrow range (by 2.8-fold). The lack of a significant increase in heterotrophic bacterial biomass within the Kerguelen bloom suggests a tight coupling between production and mortality rates. Surprisingly, HNF, the predominant grazers of bacteria, did not respond to the high abundance of active and rapidly growing bacteria at the bloom station

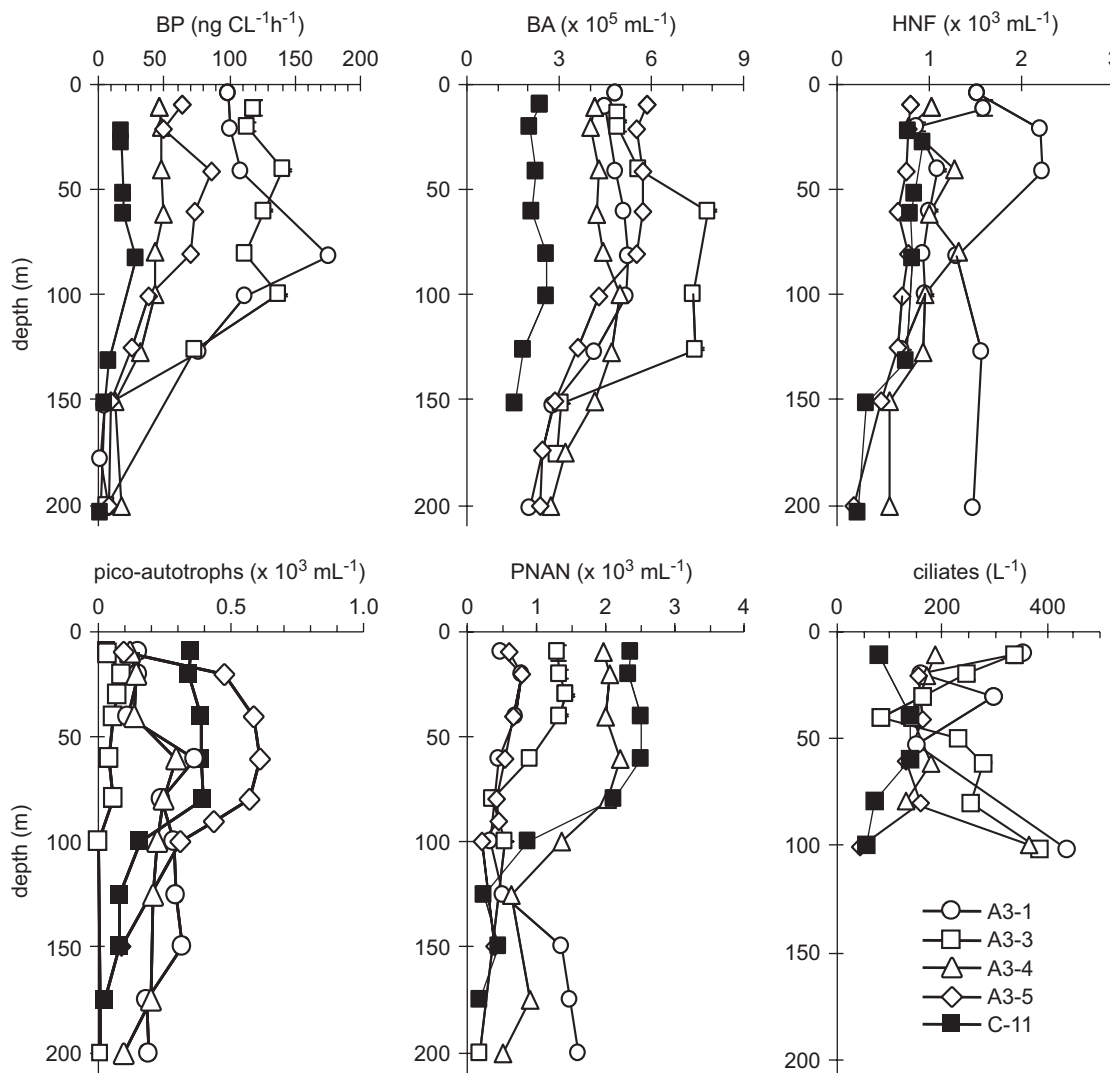


Fig. 4. Bacterial production (BP, $\text{ng CL}^{-1}\text{h}^{-1}$), bacterial (BA, $10^5\text{ cells mL}^{-1}$), heterotrophic nanoflagellate (HNF, $\text{cells } 10^3\text{ mL}^{-1}$), pico-autotroph ($\text{cells } 10^3\text{ mL}^{-1}$), phototrophic nanoflagellate (PNAN, $\text{cells } 10^3\text{ mL}^{-1}$) and ciliate abundance (cells L^{-1}) during four visits at the bloom station A3 and for one occupation at the HNLC station C11 (see also Table 1).

Table 3

Mean \pm S.D. of bacterial biomass (BACT), bacterial production (BP), biomass of heterotrophic nanoflagellates (HNF) and ciliates (CIL) at selected stations in the mixed layer (Zm)

Station	Zm (m)	BACT ($\mu\text{g CL}^{-1}$)	HNF ($\mu\text{g CL}^{-1}$)	CIL ($\mu\text{g CL}^{-1}$)
A3-1	52	5.9 ± 0.3	6.6 ± 3.6	0.95 ± 0.56
A3-3	51	7.2 ± 1.7	5.4 ± 1.4	1.7 ± 1.1
A3-4	79	5.2 ± 0.2	5.4 ± 1.1	0.6 ± 0.45
A3-5	84	7.0 ± 0.2	3.7 ± 0.3	0.52 ± 0.2
A1	83	4.9 ± 0.2	7.3 ± 1.4	1.5^a
A11	44	5.6 ± 0.1	5.9^a	nd
B5	84	4.4 ± 0.1	9.6 ± 3.0	0.82 ± 0.5
C5	77	4.0 ± 0.1	4.0 ± 1.1	1.97^a
C11	73	2.7 ± 0.2	4.1 ± 0.4	0.43 ± 0.37

$n = 6$ or 8 , nd: no data.

^aValue from 5 to 10 m depth only.

(Figs. 3 and 4, Table 3). We observed similar abundances of HNF in surface waters within and outside the bloom (Fig. 4), indicating a relatively weak predator–prey relationship at the bloom station. This is confirmed by grazing experiments that revealed an average loss of bacteria due to predation of about 35% of BP (mean of four visits at station A3) at the bloom station. In contrast, the predator–prey relationship was more important at the HNLC-site (station C11) where HNF consumed a major part of bacterial biomass (95%). The strong correlation between BP values and heterotrophic nanoflagellate stock at sites where BP was low and the absence of correlation within the phytoplankton bloom supports the idea that HNF represented a relatively weak link to higher trophic levels above the Kerguelen Plateau. Substantially higher viral abundances (3-fold) and production rates (7-fold) at

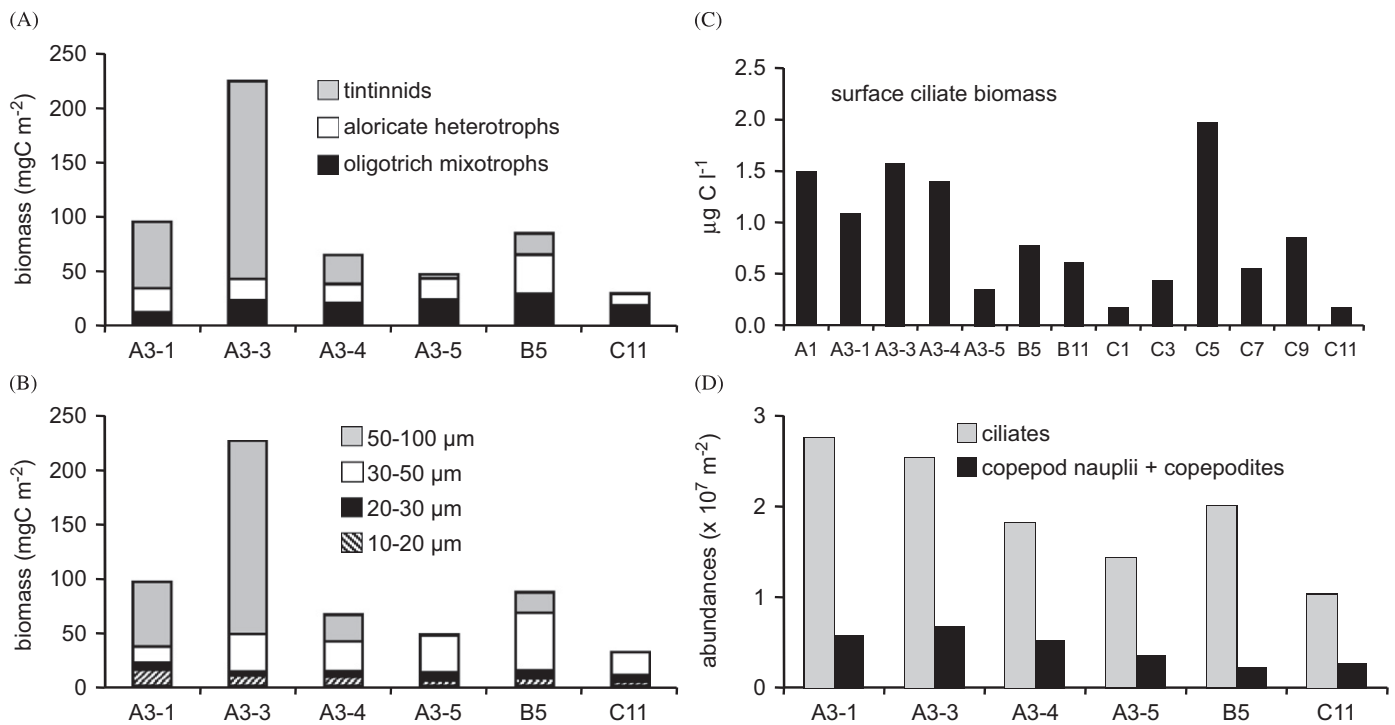


Fig. 5. Integrated ciliate biomass (0–100 m) for the three ciliate groups, tintinnids, aloricate heterotrophs and mixotrophs (A), ciliate size classes (expressed in equivalent spherical diameter) (B), ciliate biomass in surface (5 or 10 depth) (C), integrated abundances of ciliates, and copepod nauplii + copepodites (D).

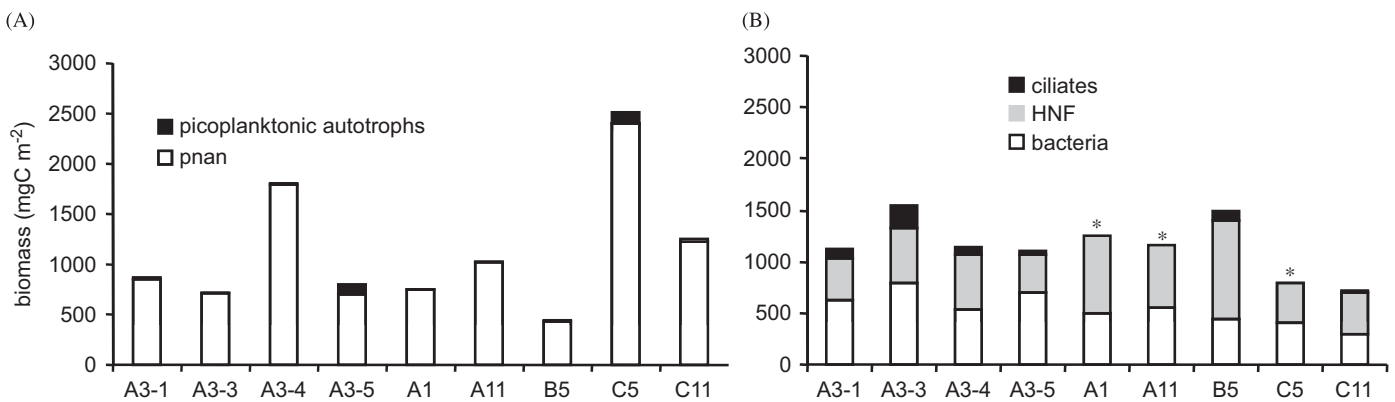


Fig. 6. Integrated biomasses of the components of the microbial food web in the 0–100 m. <math>< 10 \mu\text{m}</math> autotrophs: pico- and nanoplankton (PNAN) (A) and ciliates, heterotrophic nanoflagellates (HNF) and bacteria (B). *No ciliate profile data available.

Table 4

Mean \pm S.D. biomass of autotrophic picoplankton <math>< 2 \mu\text{m}</math> (PICO-AUTO), phototrophic nanoplankton (PNAN), % of chlorophyll a <math>< 10 \mu\text{m}</math> (Chl a) in the mixed layer depth (Zm) and % of <math>< 10 \mu\text{m}</math> primary production (PP) in the euphotic layer depth (Ze), nd: no data

Station	Zm (m)	PICO-AUTO ($\mu\text{g C l}^{-1}$)	PNAN ($\mu\text{g C l}^{-1}$)	% Chl a <math>< 10 \mu\text{m}</math>	Ze (m)	% PP <math>< 10 \mu\text{m}</math>
A3-1	52	0.15 ± 0.06	9.6 ± 2.9	11	42	15.3
A3-3	51	0.02 ± 0.01	9.5 ± 0.4	26	40	21.8
A3-4	79	0.1 ± 0.04	18.3 ± 0.8	21	46	37.5
A3-5	84	0.9 ± 0.5	8.6 ± 3.7	16	44	15.7
A1	83	0.03 ± 0.02	7.9 ± 2.5	nd	nd	nd
A11	44	0.07 ± 0.006	12.6 ± 0.9	nd	nd	nd
B5	84	0.1 ± 0.03	4.1 ± 1.1	12	40	19
C5	77	1.2 ± 0.2	26.8 ± 7.0	85	83	86.3
C11	73	0.28 ± 0.02	13.5 ± 0.8	64	98	74.7

Table 5
Comparative table between KEOPS and artificial enrichment experiments

	Chl <i>a</i>	BP	HNF	PN	BN	CIL	HNA	
IRONEX II 1995 Equatorial Pacific	x17	x3	No change	x1.7	x1.7	x3	Incr	Cochlan (2001); Landry et al. (2000a, b)
SOIREE 1999 Southern Ocean	x6	x3	x (–3)	x6	x0	x2		Hall and Safi (2001); Boyd et al. (2000)
EISENEX 2000 Southern Ocean	x4	x2 to 3			x2	x2		Arrieta et al. (2004); Gervais et al. (2002); Henjes et al. (2007)
SEEDS 2001 Subarctic Pacific	x10		x3		x1.5	x (–2)		Suzuki et al. (2005); Saito et al. (2005)
SOFEX 2002 Subarctic Pacific	x8	x2			x2		1.3	Oliver et al. (2004)
KEOPS 2005 Southern Ocean	x11.4	x12	x2.6	x (–6)	x2.8	x2.7	x4.7	Integrated 0–100 m

For KEOPS *x*-fold difference between highest and lowest integrated values (0–100) in the bloom and HNLC area. For other experiments, comparison of values inside and outside the patch. Note that the sign (–) for KEOPS indicates a highest value in the HNLC relative to the bloom area, while (–) for the other experiments indicates *x*-fold decrease after iron addition. Chlorophyll *a* (Chl *a*), bacterial production (BP), abundance of heterotrophic nanoflagellates (HNF), phototrophic nanoplankton (PNAN), heterotrophic bacteria (BACT), ciliates (CIL), high nucleic acid bacteria (HNA). incr: Increase after iron addition but no values given.

station A3 than at the HNLC-site C11 indicate that viruses had an important role in the regulation of bacterial biomass within the Kerguelen bloom (Brussaard et al., 2008; Malits, unpublished KEOPS data). These results strongly suggest top-down control of bacteria by viruses over the bloom area and the dominance of grazing control in the HNLC area. The strong positive correlation between phytoplankton biomass and BP and bacterial biomass suggests that bacteria were positively responding to phytoplankton-derived DOM creating new biomass. Bottom-up control of bacteria by phytoplankton-derived DOM also is supported by an on-board FeCl₃-enrichment experiment (Obenosterer et al., 2008). The second aspect of HNF grazing that should be considered is the possibility that the HNF somehow escaped top-down control in the HNLC area while they were subject to strong top-down control in the bloom area. Since we can measure predation on HNF we used the general model of the regulation of HNF abundance in a given system described by Gasol (1994) (Fig. 7). The model suggests that for any HNF abundance higher than that predicted by the Maximum Attainable Abundance (MAA) line, HNF predation would remove more bacterial cells than produced and would reduce bacterial abundance. The Mean Realised Abundance (MRA) line averages both types of regulation on HNF (Fig. 7). Most KEOPS data fall between MAA and MRA lines suggesting that HNF were below the carrying capacity of the system and that were mostly bottom-up controlled by bacterial availability. Moreover, similar abundances of HNF are observed within and outside the bloom. The few HNF values below the MRA line

suggesting top-down control on HNF correspond to samples below the mixed layer from the bloom area where we observed higher ciliates concentrations (Fig. 4).

During the KEOPS cruise, we observed relatively low abundances of ciliates ranging between 20 and 556 organisms l^{–1} and no major differences in abundance were detectable inside and outside the bloom. In terms of biomass, however, these two areas were distinctly different (Fig. 5). This is due to differences in the relative contribution of various size classes (Fig. 5). Large ciliates, predominantly tintinnids in the 50–100- μ m-size fraction (ESD, Table 2) dominated ciliate biomass at the bloom station in particular during the first two visits, while small aloricate ciliates, in the 30–50 μ m size class dominated at the HNLC site (Fig. 5A and B). The changes in tintinnid assemblages and biomass are attributed to food resources and their predators (Alder and Boltovskoy, 1991). In a tintinnid study in the Weddell Sea during the austral summer, Buck et al. (1992) report that *Cymatocylis* dominated open waters, while *Salpingella* was numerically dominant at the ice covered stations. Buck et al. (1992), who considered having sampled in a post phytoplankton bloom phase with well-developed open water tintinnid populations, report biomasses of the same order of magnitude as ours. They also concluded that tintinnids, in the abundance found and at reported grazing rates, could only graze a minor fraction of the primary production.

In the previous paragraph based on the model proposed by Gasol (1994) we discussed the possibility of ciliates regulating HNF abundance in the bloom stations below

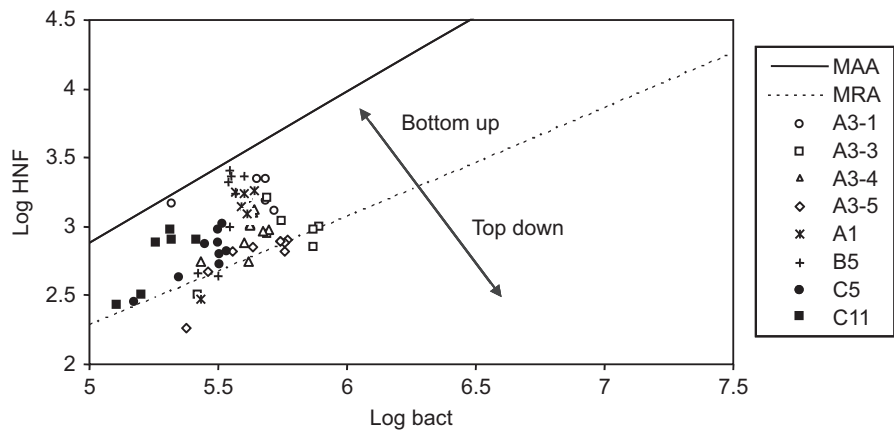


Fig. 7. Relation between log heterotrophic nanoflagellates abundance (HNF, ml^{-1}) and log bacterial prey (ml^{-1}) from the model of Gasol (1994). All HNF abundances fall below the MAA (Maximum Attainable Abundance) line (based on resources). Most of HNF fall above the MRA (Maximum Realised Abundance) for marine environment suggesting bottom-up control on HNF. HNF values below the MRA line suggesting top-down control on HNF correspond to samples in the bloom below the mixed layer where ciliate abundance increased (cf. Fig. 1). station A3 was the core of the bloom; stations A1 and B5 were influenced by the bloom stations, C5 and C11 were HNLC stations (cf. part 2.1).

the mixed layer. We will discuss now the potential of ciliates as primary production consumers. Considering that potential prey of ciliates are smaller-sized phytoplankton ($<10\ \mu\text{m}$), an estimation of the ciliate impact on nano- and picophytoplankton can be calculated based on a potential clearance rate of 10^5 body volumes h^{-1} (Fenchel, 1980; Jonsson, 1986) and the $<10\ \mu\text{m}$ primary production. Clearance rates based on 10^5 body volumes h^{-1} ranged from $0.26\ \mu\text{l cell}^{-1}\ \text{h}^{-1}$ for small conical cells ($20\ \mu\text{m}$) to $27\ \mu\text{l cell}^{-1}\ \text{h}^{-1}$ for *L. strobila* (mean 3.45, median $1.5\ \mu\text{l cell}^{-1}\ \text{h}^{-1}$). Primary production in the $<10\ \mu\text{m}$ size fraction averaged only 23% of the total primary production (Table 4) at station A3, while at station C11 the $<10\ \mu\text{m}$ size-fraction accounted for most of the primary production (72% on Table 4). Based on the clearance rate potential of ciliates and primary production in the $<10\ \mu\text{m}$ size fraction, we estimated that roughly 3% and 1.5% of the total primary production at station A3 and C11, respectively, are consumed by ciliates. Using maximum clearance rate of $10\ \mu\text{l cell}^{-1}\ \text{h}^{-1}$ (Capriulo et al., 1991; Kivi and Setälä, 1995; Dolan and McKeon, 2005), which for our data would correspond to a mean of 2.9×10^5 body volumes h^{-1} , still a small percentage of primary production (respectively, 8.7% and 4.3% for stations A3 and C11), would transit through the ciliates. The incapability of microzooplankton to consume a substantial fraction of the primary production within the phytoplankton bloom and the lack of top-down control by heterotrophic flagellates on bacteria indicates 'missing' links in terms of carbon transfer between the microbial food web and higher trophic levels (copepods). The question that can arise here is why microzooplankton organisms are not capable of biomass build-up and control over phytoplankton (Irigoien et al., 2005). One explanation supported by field observations is that the biomass of ciliates is kept in check by the grazing pressure of metazooplankton in particular copepods, which

feed preferentially on heterotrophic protists rather than on phytoplankton (e.g., Sanders and Wickham, 1993; Turner et al., 2001). In the present study, tintinnid ciliates seemed to develop related to the phytoplankton bloom (Fig. 5A) but they could not establish a dense population, suggesting that predation by mesozooplankton was high. Comparable findings of low abundances and a minor increase of total ciliates also were observed during mesoscale iron-addition experiments (Table 4). Hall and Safi (2001, SOIREE) report a moderate increase of ciliate biomass from 0.74 to $1.7\ \mu\text{g l}^{-1}$ while Boyd et al. (2004, SERIES) reported that microzooplankton grazing dramatically dropped during the peak of the bloom (≈ 5 -fold).

Copepod grazing pressure on microzooplankton during iron-addition experiments have been reported in the past (Rollwagen Bollens and Landry, 2000; Henjes et al., 2007). Copepod species composition in the KEOPS study area was dominated by large Calanidae and small Oithonidae and Oncaeidae. These taxa are known to be omnivorous, which also could explain the low abundance and biomass of ciliates inside and outside the bloom. Moreover, the copepods were characterized by a distribution in all life stage forms (nauplii, copepodites, adults), which are typical of a well-established population (Carlotti et al., 2008). This is also confirmed by our counting's in settling chambers. Although a relatively small volume of water was examined (250 ml) nauplii and copepodites were present in all samples (Fig. 5D) with a proportion of about 1 copepod to 4–5 ciliate at stations C11 and A3 and about 1 copepod to 9 ciliates at station B5.

5. Conclusions

Overall, our results demonstrate that natural iron fertilization of surface waters over a long time period (3 months) resulted in a maturation of the system, of the

Southern Ocean and had a profound impact on the microbial food web structure. The Kerguelen bloom was clearly dominated by large diatoms while the biomass contribution of small-sized phytoplankton was of minor importance. Heterotrophic bacteria responded markedly to phytoplankton activity by substantial increases in biomass production and respiration (Obernosterer et al., 2008). The lack of top-down control by HNF, however, prevented an efficient transfer of bacterial biomass to higher trophic levels. Viral lysis appeared to be the predominant control mechanism of bacterial biomass production within the Kerguelen bloom thereby returning most of the bacterial cell carbon to the dissolved pool. The low abundances of HNF and the low contribution of small-sized cells to overall phytoplankton biomass, and the probably efficient top-down control by mesozooplankton grazing prevented the biomass build-up of ciliates, the link between the microbial and the classical food webs. In HNLC-waters, a tight coupling between bacterial biomass production and HNF grazing existed. Concurrently, small-sized phytoplankton presented an important biomass component supporting biomass production of ciliates and thus a more efficient transfer of photosynthetically fixed carbon from the microbial to the classical food web.

Acknowledgments

We are grateful to the co-ordinator of the KEOPS project Dr. S. Blain for giving us the opportunity to participate in this extraordinary cruise, for the excellent conditions of work and his support during all the stages of the realization of the project. We thank Dr. D. Vaqué for her advice in preparing the minicells and the Yale University Genetic Stock Centre for providing *E. coli* x1488 free of charge. We also thank our many colleagues who participated in the collection of various data sets and in particular Dr. B. Griffith for making available his scintillation counter on-board, the officers and the crew aboard the R/V 'Marion Dufresne' for their help in the successful completion of the cruise and Dr. P. Magee for checking the English. This paper also benefited from the constructive comments of three anonymous reviewers. This work was supported by the French Research program of the INSU-CNRS PROOF and the French Polar Institute (IPEV).

References

Alder, V.A., Boltovskoy, D., 1991. Microplanktonic distributional patterns west of the Antarctic Peninsula, with special emphasis on the tintinnids. *Polar Biology* 11, 103–112.

Arrieta, J.M., Weinbauer, M.G., Lute, C., Herndl, G.J., 2004. Response of bacterioplankton to iron fertilization in the Southern Ocean. *Limnology and Oceanography* 49, 799–808.

Beers, J.R., Stewart, G.L., 1967. Microzooplankton in the euphotic zone at five locations across the California Current. *Journal of the Fisheries Research Board of Canada* 24, 2053–2068.

Blain, S., Tréguer, P., Belviso, S., Bucciarelli, E., Denis, M., Desabre, S., Fiala, M., Martin-Jézéquel, V., Le Fèvre, J., Mayzaud, P., Marty, J.C., Razouls, S., 2001. A biochemical study of the island mass effect in the context of the iron hypothesis, Kerguelen Islands, Southern Ocean. *Deep-Sea Research I* 48, 163–187.

Blain, S., Quéguiner, B., Armand, L.K., Belviso, S., Bombled, B., Bopp, L., Bowie, A., Brunet, C., Brussaard, C., Carlotti, F., Christaki, U., Shreeve, R.S., Corbière, A., Durand, I., Ebersbach, F., Fuda, J.L., Garcia, N., Gerringa, L., Griffiths, B., Guigue, C., Guillemin, C., Jaquet, S., Jeandel, C., Laan, P., Lefèvre, D., Lomonaco, C., Malits, A., Mosseri, J., Obernosterer, I., Park, H.Y., Picheral, M., Pondaven, P., Remenyi, T., Sandroni, V., Sarthou, G., Savoye, N., Scouarnec, L., Souhaut, M., Thuiller, D., Timmermans, K., Trull, T., Uitz, J., Van-Beek, P., Veldhuis, M., Vincent, D., Viollier, E., Wong, L., Wagener, T., 2007. Impact of natural iron fertilization on carbon sequestration in the Southern Ocean. *Nature* 446, 1070–1074.

Blain, S., Quéguiner, B., Trull, T., 2008. The natural iron fertilization experiment KEOPS (Kerguelen Ocean and Plateau compared Study): an overview. *Deep-Sea Research II*, this issue [doi:10.1016/j.dsr2.2008.12.002].

Børshheim, K.Y., Bratbak, G., 1987. Cell volume to cell carbon conversion factors for a bacterivorous *Monas* sp. enriched from sea water. *Marine Ecology Progress Series* 36, 171–179.

Boyd, P.W., Watson, A., Law, C.S., Abraham, E., Trull, T., Murdoch, R., Bakker, D.C.E., Bowie, A.R., Charette, M., Croot, P., Downing, K., Frew, R., Gall, M., Hadfield, M., Hall, J., Harvey, M., Jameson, G., La Roche, J., Liddicoat, M., Ling, R., Maldonado, M., McKay, R.M., Nodder, S., Pickmere, S., Pridmore, R., Rintoul, S., Safi, K., Sutton, P., Strzepek, R., Tannenberger, K., Turner, S., Waite, A., Zeldis, J., 2000. A mesoscale phytoplankton bloom in the polar Southern Ocean stimulated by iron fertilization. *Nature* 407, 695–702.

Boyd, P.W., Law, C.S., Wong, C.S., Nojiri, Y., Tsuda, A., Levasseur, M., Takeda, S., Rivkin, R., Harrison, P.J., Strzepek, R., Gower, J., McKay, R.M., Abraham, E., Arychuk, M., Barwell-Clarke, J., Crawford, W., Crawford, D., Hale, M., Harada, K., Johnson, K., Klyosawa, H., Kudo, I., Marchetti, A., Miller, W., Needoba, J., Nishioka, J., Ogawa, H., Page, J., Robert, M., Saito, H., Sastri, A., Nelson, S., Soutar, T., Sutherland, N., Taira, Y., Whitney, F., Wong, S.-K.E., Yoshimura, T., 2004. The decline and fate of an iron-induced subarctic phytoplankton bloom. *Nature* 428, 549–553.

Boyd, P.W., Jickells, T., Law, C.S., Blain, S., Boyle, E.A., Buesseler, K.O., Coale, K.H., Cullen, J.J., de Baar, H.J.W., Follows, M., Harvey, M., Lancelot, C., Levasseur, M., Owens, N.P.J., Pollard, R., Rivkin, R.B., Sarmiento, J., Shoemann, V., Smetacek, V., Takeda, S., Tsuda, A., Turner, S., Watson, A.J., 2007. Mesoscale iron enrichment experiments 1993–2005: synthesis and future directions. *Science* 315, 612–617.

Brussaard, C.P.D., Timmermans, K.R., Uitz, J., Veldhuis, M.J.W., 2008. Virioplankton dynamics and virally induced phytoplankton lysis versus microzooplankton grazing southeast of the Kerguelen (Southern Ocean). *Deep-Sea Research II*, this issue [doi:10.1016/j.dsr2.2007.12.034].

Buck, K.R., Garrison, D.L., Hopkins, T.L., 1992. Abundance and distribution of tintinnid ciliates in an ice edge zone during the austral autumn. *Antarctic Science* 4, 3–8.

Capriulo, G.M., Sherr, E.B., Sherr, B.F., 1991. Trophic behaviour and related community feeding activities of heterotrophic marine protists. In: Reid, P.C., Turley, C., Burkill, P.H. (Eds.), *Protozoa and their Role in Marine Processes*. Springer, Berlin, pp. 219–279.

Carlotti, F., Thibault-Botha, D., Nowaczyk, A., Lefèvre, D., 2008. Zooplankton community structure, biomass and role in carbon fluxes during the second half of a phytoplankton bloom in the eastern sector of the Kerguelen Shelf (January–February 2005). *Deep-Sea Research II*, this issue [doi:10.1016/j.dsr2.2007.12.010].

Church, M.J., Hutchins, D.A., Ducklow, H.W., 2000. Limitation of bacterial growth by dissolved organic matter and iron in the Southern Ocean. *Applied and Environmental Microbiology* 66, 455–466.

- Coale, K.H., Johnson, K.S., Fitzwater, S.E., Blain, S., Stanton, T.P., Coley, T.L., 2004. Southern Ocean iron enrichment experiment, carbon cycling in high- and low-Si waters. *Science* 304, 408–414.
- Cochlan, W.P., 2001. The heterotrophic bacterial response during a mesoscale iron enrichment experiment (IronEx II) in the eastern equatorial Pacific Ocean. *Limnology and Oceanography* 46, 428–435.
- Dolan, J.R., McKeon, K., 2005. The reliability of grazing rate estimates from dilution experiments: have we over-estimated rates of organic carbon consumption by microzooplankton? *Ocean Science* 1, 1–7.
- Fenchel, T., 1980. Relation between particle size selection and clearance in suspension-feeding ciliates. *Limnology and Oceanography* 25, 733–738.
- Fukuda, R., Ogawa, H., Nagata, T., Koike, I., 1998. Direct determination of carbon and nitrogen contents of natural bacterial assemblages in marine environments. *Applied and Environmental Microbiology* 64, 3352–3358.
- Gasol, J.M., 1994. A framework for the assessment of top-down vs bottom-up control of heterotrophic nanoflagellate abundance. *Marine Ecology Progress Series* 113, 291–300.
- Gervais, F., Riebesell, U., Gorbunov, M.Y., 2002. Changes in primary productivity and chlorophyll *a* in response to iron fertilization in the Southern Polar Frontal Zone. *Limnology and Oceanography* 47, 1324–1335.
- Gilron, G.L., Lynn, D.H., 1989. Assuming a 50% cell occupancy of lorica overestimates tintinnid ciliate biomass. *Marine Biology* 103, 413–416.
- Hall, J.A., Safi, K., 2001. The impact of in situ Fe fertilization on the microbial food web in the Southern Ocean. *Deep-Sea Research II* 48, 2591–2613.
- Henjes, J., Assmy, P., Klaas, C., Verity, P., Smetacek, V., 2007. Response of microzooplankton (protists and small copepods) to an iron induced phytoplankton bloom in the Southern Ocean (EisenEx). *Deep-Sea Research I* 54, 363–384.
- Irigoin, X., Flynn, K.J., Harris, R.P., 2005. Phytoplankton blooms: a ‘loophole’ in microzooplankton grazing impact. *Journal of Plankton Research* 27, 313–321.
- Jonsson, P.R., 1986. Particle feeding selection, feeding rates and growth dynamics of marine planktonic oligotrichous ciliates (Ciliophora: Oligotrichina). *Marine Ecology Progress Series* 33, 265–277.
- Kirchman, D.L., 1993. Leucine incorporation as a measure of biomass production by heterotrophic bacteria. In: Kemp, P.F., Sherr, B.F., Sherr, E.B., Cole, J.J. (Eds.), *Handbook of Methods in Aquatic Microbial Ecology*. Lewis Publishers, Boca Raton, pp. 509–512.
- Kirchman, D.L., Meon, B., Contrell, M.T., Hutchins, D.A., Weeks, D., Bruland, K.L., 2000. Carbon versus iron limitation of bacterial growth in the California upwelling regime. *Limnology and Oceanography* 45, 1681–1688.
- Kivi, K., Setälä, O., 1995. Simultaneous measurements of food particle selection and clearance rates of planktonic oligotrich ciliates (Ciliophora: Oligotrichina). *Marine Ecology Progress Series* 119, 125–137.
- Landry, M.R., Barber, R.T., Bidigare, R.R., Chai, F., Coale, K.H., Dam, H.G., Lewis, M.R., Lindley, S.T., McCarthy, J.J., Roman, M.R., Stoecker, D.K., Verity, P.G., White, J.R., 1997. Iron and grazing constraints on primary production in the Central Equatorial Pacific, an EqPac synthesis. *Limnology and Oceanography* 42, 405–418.
- Landry, M.R., Costantinou, J., Latasa, M., Brown, L., Bidigare, R.R., Ondrusek, M.E., 2000a. Biological response to iron fertilization in the Eastern Equatorial Pacific (IronEx II). III. Dynamics of phytoplankton growth and microzooplankton grazing. *Marine Ecology Progress Series* 201, 57–72.
- Landry, M.R., Ondrusek, M.E., Tanner, S.J., Brown, S.L., Costantinou, J., Bidigare, R.R., Coale, K.H., Fitzwater, S., 2000b. Biological response to iron fertilization in the eastern equatorial Pacific (IronEx II). I. Microplankton community abundances and biomass. *Marine Ecology Progress Series* 201, 27–42.
- Lebaron, P., Parthuisot, N., Catala, P., 1998. Enumeration of bacteria in aquatic systems. *Applied and Environmental Microbiology* 64, 1725–1730.
- Lebaron, P., Servais, P., Agogue, H., Courties, C., Joux, F., 2001. Does the high nucleic acid content of individual bacterial cells allow us to discriminate between active and inactive cells in aquatic systems? *Applied and Environmental Microbiology* 67, 1775–1782.
- Maldonado, M.T., Price, N.M., 1999. Utilization of iron bound to strong organic ligands by phytoplankton communities in the Subarctic Pacific Ocean. *Deep-Sea Research II* 46, 2447–2473.
- Montagnes, D.J.S., Lynn, D.H., 1991. Taxonomy of Choreotrichs, the major marine planktonic ciliates, with emphasis on the aloriccate forms. *Marine Microbial Food Webs* 5, 59–74.
- Mosseri, J., Quéguiner, B., Armand, L., Cornet-Barthau, V., 2008. Impact of iron on silicon utilization by diatoms in the Southern Ocean: a case of Si/N cycle decoupling in a naturally iron-enriched area. *Deep-Sea Research II*, this issue [doi:10.1016/j.dsr2.2007.12.003].
- Obernosterer, I., Christaki, U., Lefèvre, D., Catala, P., Van Wambeke, F., Le Baron, P., 2008. Rapid bacterial remineralization of organic carbon produced during a phytoplankton bloom induced by natural iron fertilization in the Southern Ocean. *Deep-Sea Research II*, this issue [doi:10.1016/j.dsr2.2007.12.005].
- Oliver, J.L., Barber, R.T., Smith, W.O., Ducklow, H.W., 2004. The heterotrophic bacterial response during Southern Ocean Iron Experiment (SOFEX). *Limnology and Oceanography* 49, 2129–2140.
- Pace, M.L., McManus, G.B., Findlay, S.E.G., 1990. Planktonic community structure determines the fate of bacterial production in a temperate lake. *Limnology and Oceanography* 35, 795–808.
- Pakulski, J.D., Coffin, R.B., Kelley, C.A., Holder, S.L., 1996. Iron stimulation of Antarctic bacteria. *Nature* 383, 133–134.
- Park, Y.H., Fuda, J.L., Durand, I., Naveira Garabato, A.C., 2008. Internal tides and vertical mixing over the Kerguelen Plateau. *Deep-Sea Research II*, this issue [doi:10.1016/j.dsr2.2007.12.027].
- Petz, W., 2005. Ciliates. In: Scott, F.J., Marchant, H.J. (Eds.), *Antarctic Marine Protists*. ABRIS and AAD Publishers, pp. 347–448.
- Porter, K.G., Feig, Y.S., 1980. The use of DAPI for identifying and counting aquatic microflora. *Limnology and Oceanography* 25, 943–948.
- Putt, M., Stoecker, D.K., 1989. An experimentally determined carbon, volume ratio for marine “oligotrichous” ciliates from estuarine and coastal waters. *Limnology and Oceanography* 34, 1097–1103.
- Rollwagen Bollens, G.C., Landry, M.R., 2000. Biological response to iron fertilization in the Eastern Equatorial Pacific (IronEx II). II. Mesozooplankton abundance, biomass, depth distribution and grazing. *Marine Ecology Progress Series* 201, 43–56.
- Saito, H., Suzuki, K., Hinuma, A., Takahashi, O., Fukami, K., Kiyosawa, H., Saino, T., Saino, T., Tsuda, A., 2005. Responses of microzooplankton to in situ iron fertilization in the Western Subarctic Pacific (SEEDS). *Progress in Oceanography* 64, 223–236.
- Sanders, R.W., Wickham, S.A., 1993. Planktonic protozoa and metazoan, predation food quality and population control. *Marine Microbial Food Webs* 7, 197–223.
- Schlitzer, R., 2004. Ocean Data View. <<http://www.awi-bremerhaven.de/GEOD/ODV>>.
- Sherr, B.F., Sherr, E.B., Fallon, R.D., 1987. Use of monodispersed, fluorescently labeled bacteria to estimate in situ protozoan bacterivory. *Applied and Environmental Microbiology* 53, 958–965.
- Slawyk, G., Collos, Y., Auclair, J.C., 1997. The use of ¹³C and ¹⁵N isotopes for the simultaneous measurement of carbon and nitrogen rates in marine phytoplankton. *Limnology and Oceanography* 22, 925–932.
- Smith, D.C., Azam, F., 1992. A simple economical method for measuring bacterial protein synthesis rates in seawater using ³H-leucine. *Marine Microbial Food Webs* 6, 107–114.
- Stoecker, D.K., Gifford, D.J., Putt, M., 1994. Preservation of marine planktonic ciliates, loss and cell shrinkage during fixation. *Marine Ecology Progress Series* 110, 293–299.
- Strzepek, R.F., Maldonado, M.T., Higgins, J.L., Hall, J., Safi, K., Wilhelm, S.W., Boyd, P.W., 2005. Spinning the Ferrous Wheel the importance of the microbial community in an iron budget during FeCycle experiment. *Global Biochemical Cycles* 19, GB4S26, doi:10.1029/2005GB002490.

- Suzuki, K., Hinuma, A., Saito, H., Kiyosawa, H., Liu, H., Saino, T., Tsuda, A., 2005. Responses of phytoplankton and heterotrophic bacteria in the Northwest Subarctic Pacific to in situ iron fertilization as estimated by HPLC pigment analysis and flow cytometry. *Progress in Oceanography* 64, 167–187.
- Tortell, P.D., Maldonado, M.T., Price, N.M., 1996. The role of heterotrophic bacteria in iron-limited ocean ecosystems. *Nature* 383, 330–332.
- Turner, J.T., Levinsen, H., Nielsen, T.G., Hansen, B.W., 2001. Zooplankton feeding ecology, grazing on phytoplankton and predation on protozoan's by copepod and barnacle nauplii in Disko Bay, West Greenland. *Marine Ecology Progress Series* 221, 209–219.
- Van Heukelem, L., Thomas, C.S., 2001. Computer-assisted high-performance liquid chromatography method development with applications to the isolation and analysis of phytoplankton pigments. *Journal of Chromatography A* 901, 31–49.
- Van Wambeke, F., Christaki, U., Giannakourou, A., Moutin, T., Souvemerzoglou, K., 2002. Longitudinal and vertical trends of bacterial limitation by and carbon in the Mediterranean Sea. *Microbial Ecology* 43, 113–133.
- Veldhuis, M.J.W., Kraay, G.W., 2000. Application of flow cytometry in marine phytoplankton research: current applications and future perspectives. *Scientia Marina* 64, 121–134.
- Verity, P., Robertson, C.Y., Tronzo, C.R., Nelson, J.R., Sieracki, M.E., 1992. Relationships between cell volume and the carbon and nitrogen content of marine photosynthetic nanoplankton. *Limnology and Oceanography* 37, 1434–1446.